Investigation of the implications of nitric oxide on biofilm development

Thesis Project in Systems Biology 30 ESTC

Report 2

(08-01-30 – 08-06-03)

Author
Benjamin Ulfenborg
a04benul@student.his.se
Computational Biology, 4th year

Supervisors
Magnus Fagerlind
magnus.fagerlind@his.se

Patric Nilsson
patric.nilsson@his.se

Examiner
Andreas Jansson
andreas.jansson@his.se

School of Life Sciences
Skövde University, Box 408
541 28, Skövde, Sweden

Abstract

Biofilms are communities of sessile microorganisms attached to a surface and imbedded in a matrix of extracellular polysaccharide substances. These communities can be found in diverse aquatic environments, such as in industrial pipes and in humans. By forming microcolony structures, which are highly resistant to adverse physical conditions as well as antimicrobial agents, biofilms are very problematic when associated with e.g. persistent infections. In order to find new ways of controlling biofilm growth, the processes involved in biofilm development must be investigated further. The main interest of this study is the occurrence of void formation inside biofilms. This phenomenon has been observed in several studies and has been correlated to cell death inside the microcolonies. The occurrence of cell death has recently been associated with the presence of nitric oxide in the biofilm. In this study, the implications of nitric oxide accumulation on biofilm development were investigated using an individual-based model. Specifically, the role of nitric oxide in void formation was considered. A large number of simulations were run using different parameter settings in order to determine if nitric oxide could account for the occurrence of void formation observed experimentally. The general predictions made by the model system showed agreement to some experimental data, but not to others. Sloughing, the detachment of chunks of cells from the biofilm, was observed in the majority of simulations. In some cases, the model also predicted the presence of live cells inside the voids, which has been observed experimentally.

Table of Contents

Abbreviations

EPS: Extracellular polysaccharide substances

CA: Cellular automata

IBM: Individual-based modeling

RNI: Reactive nitrogen intermediates

ROI: Reactive oxygen intermediates

NO: Nitric oxide

IDE: Integrated development environment

1 Introduction

In natural environments, bacteria predominantly live in microbial communities attached to a surface, rather than as free-living (planktonic) organisms. These sessile communities, called biofilms, can be composed of either a single or multiple microbial species. Although biofilms most often comprise multiple species, single-species communities can be found in various infections and on medical implants [1].

Bacteria are thought to attach to a surface and initiate biofilm formation as a response to certain cues in the environment. Conditions that have been implicated to influence biofilm formation include nutrient content, temperature, osmolarity, pH, iron and oxygen. Following attachment, the bacteria adapt to life as a sessile community. One of the changes that take place is the increased synthesis of extracellular polysaccharide substances (EPS) [1]. The EPS make up an extracellular matrix in which the bacterial cells become imbedded. Living in a biofilm provides the bacteria with a spectrum of benefits, including defense against hostile environmental conditions e.g. host immune responses, facilitation of growth by allowing the bacteria to remain in a favorable environment, and facilitation of cell-cell signaling and genetic exchange by allowing close association between the bacteria [2].

By utilizing cell-cell communication (e.g. quorum sensing), the bacteria in biofilms can form three-dimensional structures, called microcolonies. Cells in these structures differentiate and become very tolerant to antimicrobial agents compared to free-living bacteria. This makes the microcolonies hard to eradicate [3, 4].

During biofilm development, bacteria also carry out coordinated dispersal, involving the detachment of cells from the community. These cells convert back to planktonic bacteria and colonize new surfaces. Dispersal events involve both detachment of single cells and sloughing (detachment of larger chunks of bacteria e.g. whole microcolonies) [5]. Factors that have been associated with the coordination of dispersal include sheer stress [6], quorum sensing [7], expression of matrix-degrading enzymes [8], nutrient availability [9] and activation of a lytic bacteriophage [3].

By developing into highly resistant microcolonies and undergoing dispersal events, the bacteria in biofilms can serve as continuous reservoirs for pathogens in, for example, drinking water systems and persistent infections. It has been estimated that approximately 80 % of all treated human infections are caused by biofilms. They are also responsible for corrosive damage on metal piping. This makes biofilms very problematic in industrial and medical settings, as well as in human infections [10, 11, 12]. From this perspective, it is clear that the ability to control biofilm development would confer a wide spectrum of benefits.

One approach to study the development of biofilms is the use of mathematical models. The earliest of these models appeared in the 1970s and considered biofilms as uniform steady-state films with one-dimensional processes. Over time, the models evolved in complexity, with stratified dynamic models appearing in the 1980s and cellular automaton (CA) models in the 1990s [13]. In CA models [14, 15, 16], real world phenomena are described by a set of simple rules that mimic physical laws governing the development of a system that is discrete in time, space and state. CA models sacrifice completeness in description of physical phenomena in exchange for making these complex systems computationally tractable [17]. Despite their underlying simplicity, CA

models can exhibit very complex behavior. This makes them useful for studying biological systems, which are difficult to represent with differential equations, due to the system's spatial non-linearity [14]. When CA models are applied to biofilms, the developing structure of the microbial community is an emergent property of the system and not a model input parameter. This is because the model relies on a bottom-up approach, where the interactions within the community and between the community and its environment dictate the development of the system [13].

Another bottom-up approach to model the development of a community is called individual-based modeling (IBM). The difference between IBM and CA modeling is that IBM treats the individuals of the community as discrete entities, with their own properties e.g. biomass and history [13, 18, 19]. In this study, an individual-based model was developed to study the development of biofilms, with focus on cell death. Specifically, the accumulation of nitric oxide and the formation of hollow voids (see bellow) in biofilms were considered. A partial differential equation (PDE) was used to model the diffusion of the molecular species in the model domain.

In a review by Webb *et al.* (2003), studies concerning the multicellular organization and development of microcolonies were discussed [4]. Several of these studies reported breakdown of the EPS matrix, as well as death [3, 20] and dispersal [21, 22] of subpopulations of cells within the biofilm. This activity culminated the formation of hollow voids in the interior of the microcolonies, surrounded by non-motile bacteria. Mechanisms correlated with this process include some of the dispersal factors mentioned above, cell lysis [23], as well as oxidative and nitrosative stress [3].

One possible cue for this dispersal process is the accumulation of quorum-sensing signals [24]. In a study by Hunt *et al.* (2003) an IBM model was used to investigate the accumulation of such signal molecules [25]. Their model predicted that the signal would be present mainly in diffusion-restricted areas. These regions are also where nutrients are most likely to be depleted. Based on these results, the implications of nutrient starvation in biofilm detachment were investigated in a subsequent study. In that following study, a modified version of the same IBM model was used. The results were compared to experimental data to evaluate the model predictions. Laboratory results of confocal laser scanning microscopy showed that hollow voids formed in cell clusters of sufficient size, with the voids located in the center of the microcolonies. Correspondence was observed between the model predictions and the experimental results. In addition to hollowing of the biofilm, the model also predicted sloughing events [24].

In a study by Barraud *et al.* (2006), the implications of certain reactive nitrogen intermediates (RNI) and reactive oxygen intermediates (ROI) for dispersal were investigated in *Pseudomonas aeruginosa* (*P. aeruginosa*) biofilms. RNI and ROI are harmful molecules that can cause cellular damage. Biofilms were stained with reporter dyes seven days following inoculation of cells and examined using confocal microscopy. The results showed that high levels peroxynitrite ($ONOO^-$) correlated with cell death and dispersal inside the biofilm. The presence of $ONOO^-$, a RNI, suggested that anaerobic metabolism took place in the biofilm. Although the biofilm was grown aerobically (in the presence of oxygen), anaerobic respiration was subsequently found to occur. This was attributed to steep oxygen gradients in larger biofilms, which limits oxygen availability deeper in the biofilm. The occurrence of anaerobic respiration suggested that nitrite (NO_2^-) and nitric oxide (NO) were produced by the bacteria in the biofilm from nitrate (NO_3^-)

in the growth medium. Since NO is the main precursor of $ONNO^-$, the role nitric oxide in biofilm dispersal was investigated further. This was done by comparing the development of mature biofilms of three strains of *P. aeruginosa*, namely wild type, a NO_2^- reductase-deficient mutant (unable to produce NO) and NO reductase-deficient mutant (unable to reduce NO). While the wild type behaved normally (hollowing occurred), the NO_2^- reductase-deficient strain showed no patterns of cell death or lysis. The NO reductase-deficient strain, on the other hand, displayed enhanced patterns of cell death and formation of numerous hollow voids inside the biofilm. From these results it was concluded that NO, or its reactive derivatives, mediated cell death and dispersal in the biofilm. In addition, it was observed that exposing 1-day-old established biofilms to sub-lethal concentrations of NO reversed biofilm formation and resulted in detachment of the bacteria from the surface [26].

From the above observations, the following hypothesis was formulated. Initially, the bacteria in a biofilm utilize aerobic respiration, as oxygen from the bulk liquid is present throughout the microcolonies. As the biofilm grows, oxygen is depleted in the deeper regions, resulting in the switch to anaerobic respiration. By consuming nitrate and nitrite, nitric oxide is produced. When the production exceeds the reduction, nitric oxide accumulates. When the bacteria experience prolonged exposure to higher levels of NO, cellular damage accumulates and eventually results in cell death. This leads to hollowing of the microcolonies.

The aim of the present study is to test this hypothesis by investigating the implications of nitric oxide production on biofilm development using an individual-based model in combination with partial differential equations. Biofilms are simulated to grow in low levels of oxygen to promote oxygen limitation deeper in the biofilm. Simulations with different parameter settings were run in order to test if nitric oxide, and the resulting damage, can account for the patterns of hollow void formation in biofilms observed experimentally [3, 21, 23, 24, 26, 27].

2 Model Description

The following sections will describe the individual-based model conceived to study the effects of nitric oxide on biofilm development. The individual bacteria will be considered to be discrete entities growing on a surface composed off discrete elements. By consuming the substrates in the environment, the bacteria accumulate biomass and develop into a biofilm attached at the substratum. As substrates are consumed, concentration gradients form which lead to lower levels of substrate in deeper regions of the biofilm. The bacteria divide when their biomass exceeds a given threshold and die when they have sustained a certain amount of damage for a specified number of time steps. Time in the model is iterated in discrete steps of one hour.

2.1 Simulation domain

The environment in which biofilm development takes place is simulated by a two-dimensional grid (lattice) of discrete cubic elements. Each side l of an element is taken to be 3 µm in length, giving an elemental size of 27 μm^3. This has been stated to be an appropriate space for containing a bacterial cell and its extracellular components [28]. Further, the number of elements x along the x-axis has been set to 300 (giving a width of 900 µm) and the number of elements y along the y-axis to 100 (giving a height of 300 µm).

All elements of the lattice are initially filled will bulk liquid, which is the aqueous solution of the environment. Upon running a simulation, the domain is seeded with a specified number of bacteria. These bacteria are assumed to attach the substratum (the lowest row of elements in the lattice). Attachment (colonization) is explained further bellow. Above the topmost bacterium of the biofilm, there is a mass transfer boundary layer of specified thickness b_t. This liquid layer separates the biofilm from the bulk phase, which extend from the top of the boundary layer to the highest row in the model domain. The boundary layer and the bulk phase will be further explained in section on molecular diffusion.

In order to avoid domain edge effects on biofilm growth, the x-axis is assumed to be continuous. This means that the left and right edges of the lattice are connected. A graphical representation of the model domain can be found in figure 1.

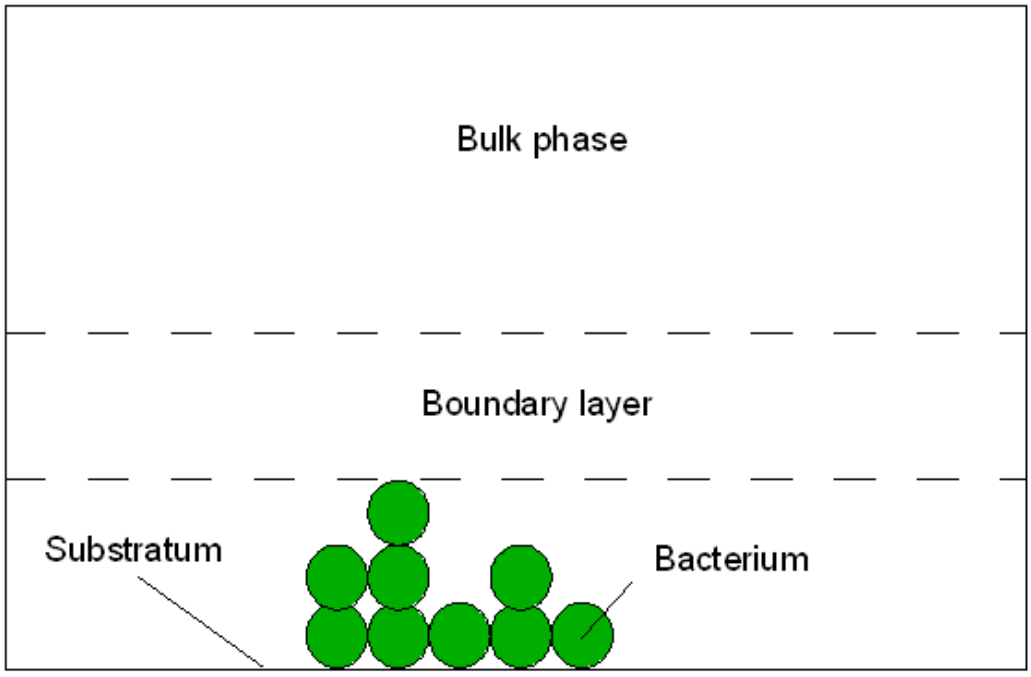

Figure 1: Simplified graphical representation of the model domain. The figure was drawn out of scale for demonstrational purposes.

2.2 Aerobic and anaerobic respiration

The bacteria in the model are assumed to be able to carry out both aerobic and anaerobic respiration. Two substrates are assumed to be limiting in this model, oxygen and nitrite. Because aerobic respiration (using oxygen as the terminal electron acceptor) yields more energy than anaerobic respiration (using nitrate or nitrite as the terminal electron acceptor) [2], the bacteria use oxygen as long as it is available. When it becomes limiting (falls bellow a specified concentration threshold), it is assumed that they gradually compensate for oxygen depletion by utilizing nitrite instead. This is based on the observation that anaerobic respiration has been found to occur in aerobically grown biofilms [26]. The reason why nitrite was chosen over nitrate is that nitrite is the direct precursor of nitric oxide, which is the molecular species of interest in this study. Support for the idea that aerobic and anaerobic can occur simultaneously comes from observations by Chen *et al.* (2005) [29]. The switch between aerobic respiration and anaerobic respiration is determined by equation 1.

$$R_{an} = \begin{cases} 0 \quad if \quad c_{rst} >= C_{O2} \\ \dfrac{c_{rst} - C_{O2}}{c_{rst}} \quad if \quad c_{rst} < C_{O2} \end{cases} \tag{1}$$

The anaerobic ratio R_{an} denotes the extent (from zero to 100 %) to which anaerobic respiration is utilized. This is calculated each time step for each bacterium. As long as the oxygen concentration C_{O2} is above the respiration switch threshold c_{rst}, only aerobic respiration will be carried out (R_{an} will be zero). When C_{O2} drops bellow c_{rst}, however, utilization of nitrite will gradually increase as R_{an} increases from zero to one. The reduction of nitrite will subsequently lead to accumulation of nitric oxide.

Since R_{an} describes the extent of anaerobic respiration utilization, it must always take on a value between zero and one (zero and 100 % utilization), no matter what value c_{rst} takes. Placing the threshold c_{rst} in the denominator in equation 1 ensures this.

2.3 Molecular diffusion

Each element in the lattice has its own concentration of oxygen, nitrite and nitric oxide. Diffusion of each molecular species across the domain is calculated once each time step. Because oxygen, nitrite and nitric oxide are all very small molecules, it is assumed that they can reside in lattice elements harboring a bacterium without any complications. The liquid of the lattice extending from the top row down to the boundary layer is called the bulk phase. This phase represents the liquid flowing into the model domain, continuously supplying nutrients for the bacteria. At each time step, the concentrations of the substrates (oxygen and nitrite) for all elements in the bulk phase are set to the specified bulk phase concentrations $C_{O2\,bulk}$ and $C_{NO2\,bulk}$ respectively. This “seeding” of the bulk phase corresponds to the influx of nutrients via the liquid into the model domain. As

molecular diffusion is carried out, the concentration of the substrates throughout the lattice depends on the bulk phase concentrations of oxygen and nitrite and on their consumption by the bacteria. Equation 2 describes the diffusion of oxygen and nitrite across the two-dimensional lattice [30].

$$\frac{\partial C_S}{\partial t} = D_S \cdot \left(\frac{\partial^2 C_S}{\partial x^2} + \frac{\partial^2 C_S}{\partial y^2} \right) - r_S(C_S, X) \tag{2}$$

The concentration of a substrate (either oxygen or nitrite) is denoted by C_S, while D_S is the diffusion rate of the substrate and r_S the consumption rate as a function of biomass density (X) and C_S. Because the biofilms' density is higher than that of the aqueous environment, diffusion of the substrate in the biofilm is more restricted. To get the diffusion rate in the biofilm, therefore, the substrate diffusion rate in aqueous phase $D_{S\,aq}$ is multiplied with the relative effective diffusivity $D_{S\,e} / D_{S\,aq}$ of the substrate [31]. $D_{S\,e}$ denotes the effective diffusion coefficient in the biofilm.

In a study by Picioreanu *et al*. (1999), the diffusional time constant was estimated to be about 100 magnitudes smaller than that for bacterial division [32]. In other words, the time frame needed for diffusion to reach steady state is much smaller than for a bacterium to divide. Based on this, it can be assumed that the concentrations of all molecular species across the lattice maintain quasi steady states with respect to bacterial division [30]. This simplification means that diffusion can be solved explicitly in sub-time (Δt) steps once each full time step until the concentration of each molecular species has reached a quasi steady-state [32]. The Δt used for oxygen diffusion is $2.9 \cdot 10^{-7}$ h and the one for nitrite and nitric oxide $4.5 \cdot 10^{-7}$ h. Once quasi steady state has been reached, all bacteria-associated processes, like consumption of substrate and division (see bellow), are carried out.

As mentioned above, the bulk phase (where the substrates are continuously seeded) and the biofilm are separated by a mass transfer boundary layer. In the mass transfer boundary layer, and through the biofilm, concentration gradients are established as a result of substrate transport from the bulk phase and substrate consumption by the bacteria. In reality, the thickness of the boundary layer depends on the liquid flow pattern in the bulk phase [33]. The present model, however, assumes that the layer's thickness b_t is constant. As Figure 1 illustrates, the layer extends a certain number of elements from the topmost bacteria in the model domain to the bulk phase.

Nitric oxide, which is not present in the bulk phase, is produced by nitrite reduction in bacteria carrying out anaerobic respiration. Since the reduction of one nitrite molecule leads to one nitric oxide molecule [29], the production of NO each time step is described by equation 3.

$$C_{NO\ prod} = \frac{Q_{NO2} \cdot m_{NO}}{m_{NO2}} \tag{3}$$

The concentration of produced nitric oxide is denoted by $C_{NO\ prod}$. The value of Q_{NO2} is the amount of nitrite consumed in a sub-time step (quasi consumption) divided by the volume of a lattice element. This means that the amount of NO produced is directly proportional to the amount of NO_2 consumed. The value of Q_{NO2} is multiplied by the mass of a nitric oxide molecule m_{NO} and divided by the mass of a nitrite molecule (m_{NO2}) to convert the mass of consumed NO_2 to the mass of produced NO.
Nitric oxide is further reduced to nitrous oxide (N_2O) in all lattice elements that harbor bacteria by the enzyme NO reductase [2]. This reduction is assumed to follow equation 4.

$$C_{NO\ red} = r_{NO} \frac{C_{NO}}{K_{NO} \cdot C_{NO}} \tag{4}$$

The concentration of reduced NO is symbolized by $C_{NO\ red}$. Nitric oxide is assumed to be given by a reduction constant r_{NO} multiplied by $\frac{C_{NO}}{K_{NO} \cdot C_{NO}}$, where C_{NO} is the NO concentration and K_{NO} denotes the concentration of NO that leads to half-saturation of the NO reductase capacity of a bacterial cell.

The diffusion of nitric oxide is described by equation 2 without the reaction term, since NO is not consumed. Like oxygen and nitrite diffusion, it is also carried out in sub-time steps until quasi steady state is reached. Together, equation 3 and 4 describe the net change in nitric oxide content each sub-time step.

2.4 Substrate consumption

As mentioned above, the bacteria are assumed to carry out both aerobic and anaerobic metabolism, depending on the concentration of oxygen and specified respiration switch threshold. For aerobic respiration, the consumption of oxygen is described by equation 5 [34].

$$r_{O2}(C_{O2}, X) = g \cdot X \cdot \left(\frac{C_{O2}}{K_{O2} + C_{O2}} \right) \tag{5}$$

The consumption rate, r_{O2}, denotes the amount of oxygen consumed. This depends on two variables: the local concentration of oxygen C_{O2} in the lattice element and the biodensity X of the bacterium. The biodensity is equal to the bacterium's biomass divided by the lattice element volume. The two constants of the equation are the growth constant g and the oxygen half-saturation coefficient K_{O2}. The growth constant is calculated according to equation 6.

$$g = \frac{\mu_{\max}}{Y_{XNO2}} + m \tag{6}$$

The three constants in this equation are the maximum growth rate $\mu_{\max}$, the oxygen yield coefficient Y_{XNO2} and the maintenance coefficient m.

The consumption of nitrite in anaerobic respiration is described by the same basic equation with an additional factor, as can be seen in equation 7.

$$r_{NO2}(C_{NO2}, X) = g \cdot X \cdot \left(\frac{C_{NO2}}{K_{NO2} + C_{NO2}} \right) \cdot R_{an} \tag{7}$$

The additional factor, R_{an} from equation 1, denotes the extent to which anaerobic respiration is utilized. This factor becomes greater than zero as the oxygen concentration falls bellow the respiration switch threshold and become 1 when oxygen is depleted.

When a substrate is consumed by a bacterium, the bacterium grows and accumulates biomass according to equation 8 [34].

$$BM_{new} = BM_{previous} + Y_{XS} \cdot r_S(C_S, X) - m \cdot X \tag{8}$$

The biomass each time step is denoted by BM_{new} and is calculated based on the biomass of the previous time step $BM_{previous}$. In the first time step, $BM_{previous}$ is $1.5*10^{-13}$ for all bacteria. The constants Y_{XS}, r_S and C_S are the yield coefficient, consumption rate and local concentration respectively, of the substrate consumed. As above, m denotes the maintenance coefficient and X the bacterial biodensity. Change in biomass is determined by the difference between biomass accumulation (from substrate consumption) and reduction (from maintenance).

2.5 Bacterial division

All bacteria start with an initial biomass of m_{ini}. If a bacterium consumes enough substrate to outweigh the loss from maintenance, the biomass of the bacterium increases. When the biomass exceeds a specified division threshold m_{div}, the bacterium divides. Upon division, the lattice is searched from the dividing bacterium until at least one element is found that does not harbor a bacterium. In other words, the closest empty element to the dividing bacterium is determined. If more than one empty element *e* is found at the same distance, an empty element is selected randomly.

There are eight neighboring elements of the dividing bacterium. The neighboring element *n* that is nearest to the chosen empty element *e* is subsequently chosen as the element where the daughter cell will be placed. The daughter cell is always placed next to the dividing bacterium. If the chosen neighboring element is occupied (i.e. if *n* is not *e*), bacteria will be shoved in order to free the chosen neighboring element *n*. The shoving

involves moving each bacterium in a strait line by one element, starting at an empty element and ending at element to free. If *e* and *n* are aligned along either the x-axis or the y-axis, the bacteria will be shoved from *n* to *e* directly. When there is no alignment, bacteria will first be shoved towards *e* from an intermediate element *i*, and then from *n* to *i*. This division algorithm means that the daughter cell will be placed in direction that offers the least mechanical resistance. A smaller number of bacteria to be shoved mean less resistance [15]. One of the daughter cells will remain in the same element after division. The dividing bacterium is assumed to split itself in two and dividing its biomass and damage equally between the two resulting cells. Figure 2 gives a graphical example if a bacterial division.

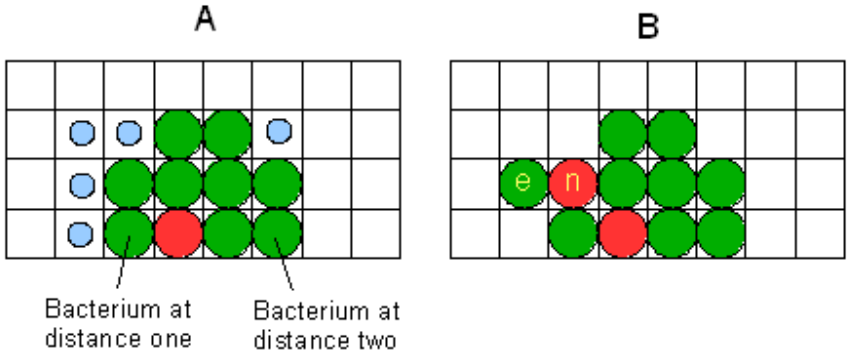

Figure 2: Graphical example of division. Panel A shows the state of the model domain before division, while panel B shows the state following division. The model domain in the figure is very small for demonstrational purposes. Green dots represent non-dividing bacteria, red dots symbolize the dividing bacterium and daughter cells, and blue dots indicate empty elements *e* at the same distance from the dividing bacterium. Since there is no empty element next to the dividing bacterium, shoving will be necessary. Because there is more that one empty element at the same distance from the dividing bacterium in panel A, one is selected randomly.

2.6 Bacterial death

As mentioned above, when the oxygen concentration drops bellow c_{rst}, a bacteria starts to utilize anaerobic respiration. The reduction of nitrite leads to the accumulation of RNI, e.g. nitric oxide and peroxynitrite, which cause cellular damage and can lead to cell death if the damage becomes too sever [25]. In the present model, it is assumed that the presence of nitric oxide leads to accumulation of damage proportional to the concentration of NO. The accumulation of damage is described by equation 9.

$$D_{new} = D_{previous} + a_{NO} \cdot C_{NO} \cdot v_e - d_r \cdot D \tag{9}$$

The damage each time step is denoted by D_{new} and is calculated based on the damage of the previous time step $D_{previous}$. In the first time step, $D_{previous}$ is zero for all bacteria. The rate of damage accumulation is a_{NO}, the concentration of nitric oxide is C_{NO} and v_e is the lattice elemental volume. Damage is removed by the bacterium's cell repair

machinery at a rate proportional to the amount of damage with a constant rate d_r. Change in damage is determined by the difference between damage accumulation (from nitric oxide) and removal (from cellular repair).

At each time step, the damage of each bacterium is compared to a specified survival threshold s_t. If the threshold is exceeded, the bacterium's death counter is increased by one. The death counter is subsequently compared to a specified survival time limit s_{tl}. If the time limit has been reached, the bacterium dies. This is modeled by removing it from the model domain.

2.7 Bacterial detachment

Two forms of bacterial detachment from the biofilm are taken into account in the present model. The first is detachment by hydrodynamic sheer stress exerted by the bulk flow on the bacteria at the biofilm surface. This was implemented according to the approach of Hermanowicz (2000), who described this detachment by the formula found in equation 10 [35].

$$P_D = \frac{1}{1+\left(\frac{B_S}{S_S}\right)} \tag{10}$$

The probability P_D that a bacterium exposed to bulk liquid will detach is a function of biofilm "strength" B_S and the sheer stress S_S. Increased strength will thus yield lower probabilities of detachment. In the present model, determination of the strength of the biofilm is simplified by assuming it to be constant.

Unlike Hermanowicz (2000), who assumed a constant sheer stress regardless of bacterium position, sheer stress in the present model depends on bacterium height over the substratum. Bacteria that are located in higher regions of the biofilm are exposed to higher sheer stress than those closer to the substratum. Specifically, the sheer stress exerted on a bacterium is assumed to be equal to the number of lattice elements from the substratum to the bacterium. Bacteria at the substratum have a sheer stress of 1. Biofilm strength is taken as a parameter to the model.

In order to detach by sheer stress, a bacterium must be exposed to the bulk liquid, i.e. the liquid outside the biofilm. This means that bacteria in the interior of the biofilm have no chance to detach by sheer stress. Although all bacteria are given a sheer stress value for convenience, it is only the outmost bacteria that actually can detach.

The second mechanism by which bacteria can detach is by losing connection to the substratum. If any of bacteria lose their last connection to the substratum as a result of bacterial death or detachment, they are pulled away by the bulk flow. For this to occur, however, the bacteria need to have at least one connection to the bulk liquid. Bacteria that lose their connection to the substratum inside the biofilm will thus not be pulled away. This form of detachment accounts for the phenomenon of sloughing, since larger chunks

of bacteria can detach simultaneously. Sloughing is simplified by removing the bacteria from the model domain immediately after connection is lost.

2.8 Parameter values

The default set of parameter values used to run simulation can be found in Table 1, along with their corresponding units and references. While several values have been experimentally determined and used by others, some had to be estimated. Regarding substrate consumption, the yield coefficient of nitrite Y_{XNO2} was given a value based on guidelines. The value for the yield coefficient for oxygen used, 0.24 g_X g_S^{-1}, was adopted from [36]. Based on estimation by Chen *et al*. (2006) that the energy yield from denitrification (anaerobic respiration) is approximately 69 % of that from aerobic respiration [29], Y_{XNO2} was estimated to be $0.24 \cdot 0.69 = 0.16$ g_X g_S^{-1}. The parameters in Table 1 without a reference were estimated by hand.

Table 1: Default parameter values used in the model

Parameter	Symbol	Value	Unit(s)	Reference
Number of elements in X	x	300	-	-
Number of elements in Y	y	100	-	-
Number of time steps	t_s	150	h	-
Save interval	t_{int}	1	h	-
Length of one side of a cubic surface element	l	$3*10^{-6}$	m	[28]
Diffusion rate of O_2	D_{O2}	$7.2*10^{-6}$	m^2 h^{-1}	[31]
Diffusion rate of NO	D_{NO}	$18.36*10^{-6}$	m^2 h^{-1}	[37]
Diffusion rate of NO_2^-	D_{NO2}	$6.12*10^{-6}$	m^2 h^{-1}	[31]
Bulk concentration of O_2	$C_{O2\,bulk}$	4	g m^{-3}	-
Bulk concentration of NO_2^-	$C_{NO2\,bulk}$	5	g m^{-3}	-
Thickness of the mass transfer boundary layer	b_t	$27*10^{-6}$	m	-
Relative effective diffusivity of O_2 in the biofilm	$D_{O2,e}/D_{O2,aq}$	0.55	-	[24]
Relative effective diffusivity of NO in the biofilm	$D_{NO,e}/D_{NO,aq}$	0.6	-	[31]
Relative effective diffusivity of NO_2^- in the biofilm	$D_{NO2,e}/D_{NO2,aq}$	0.6	-	[31]
Interval for the search for quasi steady state of molecular diffusion	-	1000	-	-
Relative error margin for quasi steady state of molecular diffusion	-	$5*10^{-4}$	-	-
Respiration switch threshold	c_{rst}	1	g m^{-3}	[38]
Number of initial bacterial cells	n_{bac}	3	-	-

Biomass of initial bacteria	m_{ini}	$1.5*10^{-13}$	g	-
Maximum growth rate	$\mu_{\max}$	0.3	h^{-1}	[24]
Yield coefficient of O_2	Y_{XO2}	0.24	$g_X\ g_S^{-1}$	[24]
Yield coefficient of NO_2^-	Y_{XNO2}	0.16	$g_X\ g_S^{-1}$	-
Maintenance coefficient	m	0.036	$g_S\ g_X^{-1}\ h^{-1}$	[39]
Half-saturation coefficient of O_2	K_{O2}	1.2	$g\ m^{-3}$	[38]
Half-saturation coefficient of NO_2^-	K_{NO2}	10.9	$g\ m^{-3}$	[40]
Survival threshold	s_t	$1*10^{-15}$	g	-
Survival time limit	s_{tl}	1	h	-
Damage removal coefficient	d_r	0.2	h^{-1}	-
Division threshold	m_{div}	$2.63*10^{-13}$	g	-
Biofilm strength	B_S	200	-	-
Reduction constant of NO	r_{NO}	0.3	$g\ m^{-3}$	-
Half-saturation coefficient of NO	K_{NO}	1	$g\ m^{-3}$	-
Damage coefficient of NO	a_{NO}	$1.4*10^4$	h^{-1}	-

2.9 Colonization

Every simulation begins with seeding the model domain with a number of bacteria. This is done by either randomly placing bacterial cells, or force-placing bacteria in certain positions, along the lowest row of the lattice (along the substratum). Force-placing is useful to avoid clustering of the initial bacteria, such that they do not form a single chunk, but develop into separate microcolonies. This was done for the majority of simulations with different parameter settings to make them easier to compare.

2.10 Simulation steps

Each simulation is carried out in discrete time steps of one hour. During each time step, a sequence of processes are carried out to model bacterial division, death etc. (Fig 3). This sequence is as follows: (1) Initialization of the model, including creating the model domain and colonization with initial bacteria. (2) Start of the simulation loop, where the time-step variable is checked against the time-step parameter t_s. If the variable is smaller, the simulation continues to step 3 (Fig 3), otherwise the simulation is terminated. (3) Diffusion of the molecular species is carried out, one at a time, until quasi steady-state has been reached. (4) Consumption of substrate by the bacteria; aerobic respiration is carried out and anaerobic if the oxygen level is bellow c_{rst}. (5) Bacterial division; each bacterium's biomass is checked against the division threshold m_{div}. If the biomass is higher, the bacterium divides. (6) Damage accumulation; each bacterium sustains a certain amount of damage depending on the concentration of nitric oxide in the element

in which the bacterium resides. (7) Bacterial death; each bacterium's damage is first checked against the survival threshold s_t and then the death counter against the survival time limit s_{tl}. If the second check turns out to be true, the bacterium dies. (8) Detachment by sheer stress; each bacterium's detachment probability is checked against a random number from zero to one. If the number is smaller than the probability, the bacterium detaches by sheer stress. (9) Detachment by lost connection; each bacterium is checked for connection to the substratum. If the connection is false and the bacterium is connected to the bulk liquid, the bacterium detaches by lost connection. (10) The state of the model domain is saved, if a specified number of time steps t_{int} have passed since the last save. The loop then returns to step 2. A graphical representation of the model can be found in Figure 3.

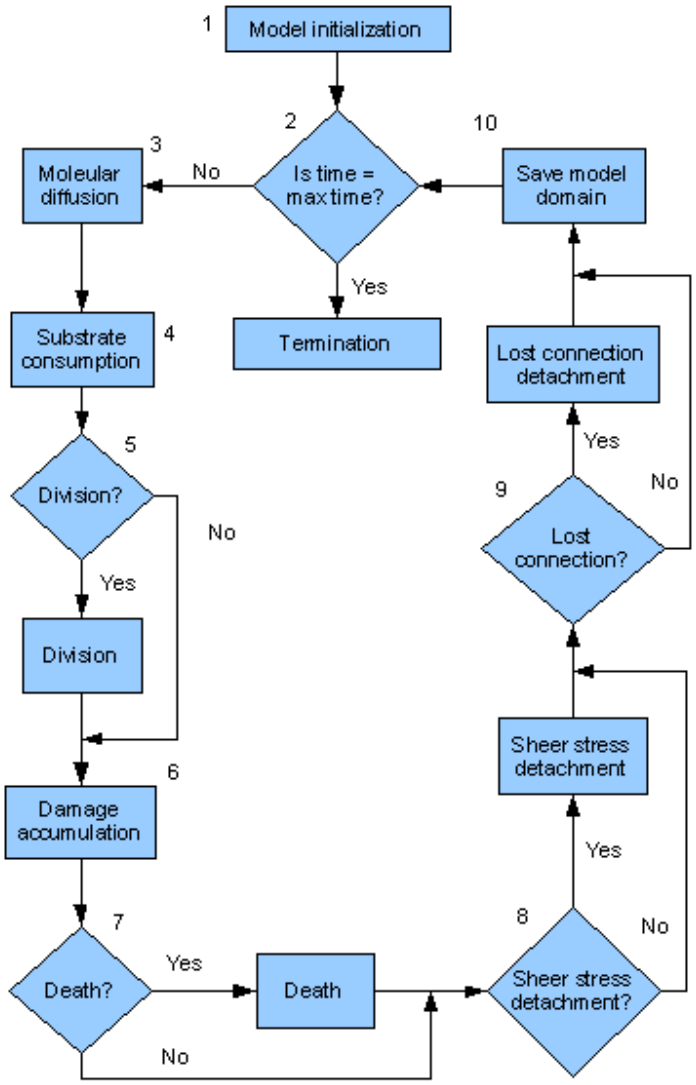

Figure 3: Graphical representation of the model. Boxes indicate computational processes and diamonds symbolize condition checks.

2.11 Simulation experiments

Because many model parameters had to be estimated by hand, initial simulations were run with a vide variety of different parameter settings. From the results of these simulations, four parameters were chosen for systematic analysis. A second set of simulations were subsequently run where each of these parameters, s_t, s_{tl}, c_{rst} and r_{NO}, were varied over a selected range of values. These simulations constitute the investigation of the implications of nitric oxide accumulation on biofilm development.

The source code of the model was written in C++ and compiled in the Dev C++ editor, a free integrated development environment (IDE) from Bloodshed Software. The results where visualized using Matlab 7.1.

3 Results & Discussion

The results obtained from the model simulations are presented bellow. While quantitative data from all simulations in the second set can be found in Table 2 to 4, only one simulation was chosen to graphically illustrate a number of observations. The values in the tables are derived from simulations that were performed with force-placed bacteria, whereas the figures show simulations with randomly placed bacteria.

3.1 Biofilm life cycle

In this section, the general characteristics of biofilm development predicted by the model will be addressed. Although differences were observed between simulations with different parameter settings, some features were common to all. Figure 4a displays the biofilm growth of a simulation run with the following setting: high survival threshold, low survival time limit, average NO reduction constant and average respiration switch threshold.

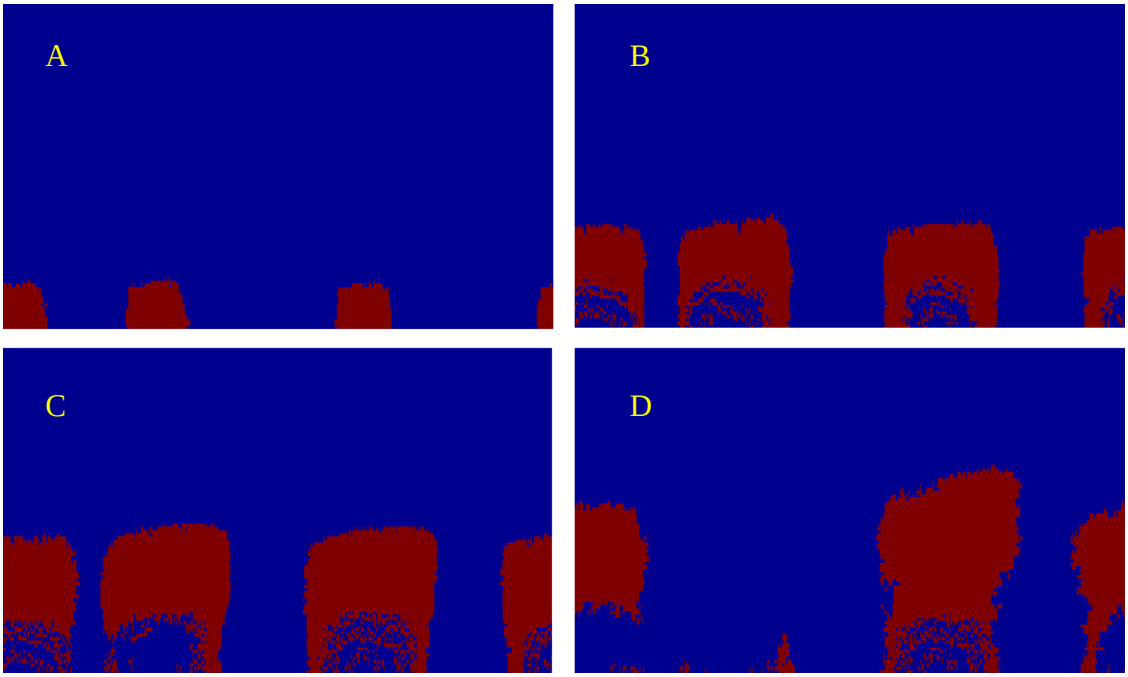

Figure 4a: Biofilm development during a simulation of 150 hours with three initially randomly placed bacteria. The left and right borders are continuous. Panel A, B, C and D picture the biofilm after 50, 75, 100 and 143 hours respectively, following colonization. Blue indicates liquid while red symbolizes the bacteria. The parameters under consideration were the survival threshold, survival time limit, nitric oxide reduction constant and respiration switch threshold. These were set to $1.5*10^{-15}$, 1, 0.3 and 1 respectively.

The pattern of development illustrated in Figure 4a shows several general features observed in the majority of simulations. Following colonization of the substratum, the initial bacteria slowly develop into microcolonies. As the microcolonies get larger, their growth is accelerated as there are more bacteria dividing. If two initial bacteria attach close enough to each other, the microcolonies may merge into a single structure. This did not occur in the simulation shown in Figure 4a, but the two leftmost microcolonies grew close enough together to form a narrow liquid channel between them.

After 70 hours in the simulation (panel B in Figure 4a), hollow voids had started to form in the three microcolonies. As in all simulations where hollowing was observed, cell death started in the deepest region of each colony. Initial voids were always located centrally in the biofilm, at the substratum. If two microcolonies grew close enough together, the voids formed near the channel between the colonies. This can be seen in panel B and C in Figure 4a.

Another observation that could often be made was the presence of live cells in the voids. This can be seen in panels B, C and D in Figure 4a. When the voids opened to the bulk liquid outside the microcolonies as a result of extensive cell death, free cells in the voids evacuated the interior of the microcolonies.

In the simulations that hollowing was observed, sloughing events generally followed. This occurred when the “legs” connecting the top of a microcolony to the substratum were severed by cell death. By comparing panel C and D in Figure 4a, a sloughing event can be confirmed in one of the microcolonies. In the majority of cases, sloughing events left behind a small group of live bacteria attached to the substratum that

subsequently developed into new microcolonies. Though the timing of sloughing differed for different parameter settings, the pattern for this detachment mechanism was similar for all simulations in which it occurred.

In Figure 4b, the oxygen gradient corresponding to the biofilm in Figure 4a can be seen.

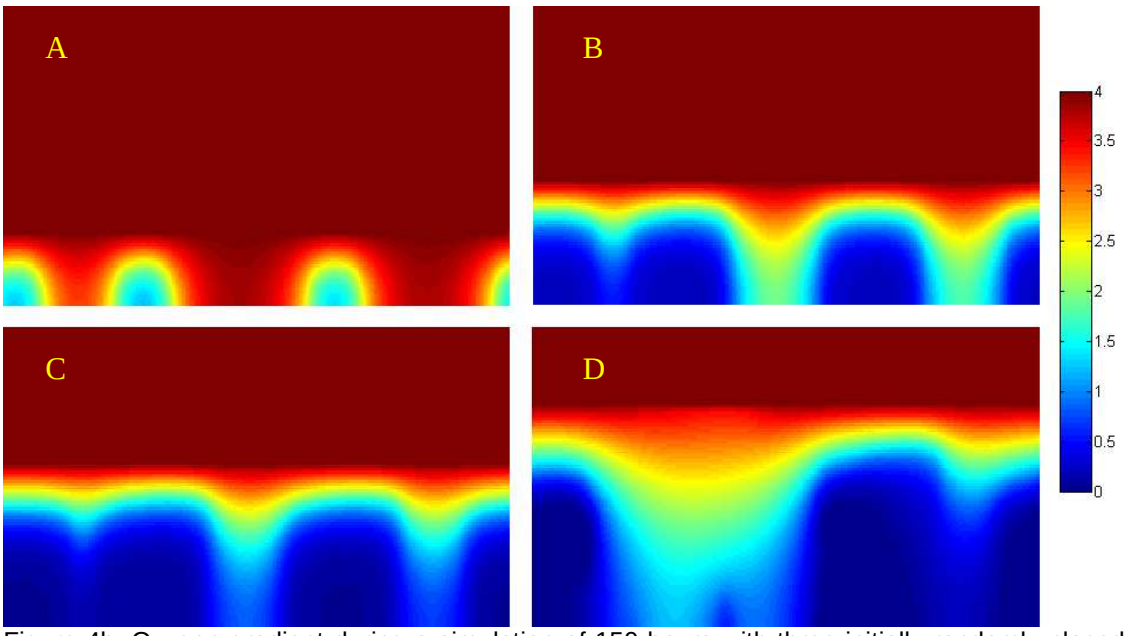

Figure 4b: Oxygen gradient during a simulation of 150 hours with three initially randomly placed bacteria. The left and right borders are continuous. Panel A, B, C and D picture the biofilm after 50, 75, 100 and 143 hours respectively, following colonization. The bar to the right indicates oxygen concentration in grams per cubic meter. The parameters under consideration were the survival threshold, survival time limit, nitric oxide reduction constant and respiration switch threshold. These were set to $1.5*10^{-15}$, 1, 0.3 and 1 respectively.

Initially, the entire model domain is set to the bulk phase oxygen concentration, so every element in the lattice will have the same concentration. As the biofilm grows, however, oxygen is consumed and a gradient forms in the microcolony. Outer bacteria will have access to a higher level of oxygen than bacteria deeper in the colonies. The establishment of the concentration gradient can be observed over time in Figure 4b from panel A through D. Eventually, the oxygen concentration will drop bellow the specified respiration switch threshold in the interior of the microcolonies. When this happens, anaerobic respiration will kick in to compensate for oxygen limitation. Depletion of oxygen in the lower parts of the biofilm was observed in all simulations performed.

Figure 4c shows the accumulation of nitric oxide in the biofilm pictured in Figure 4a.

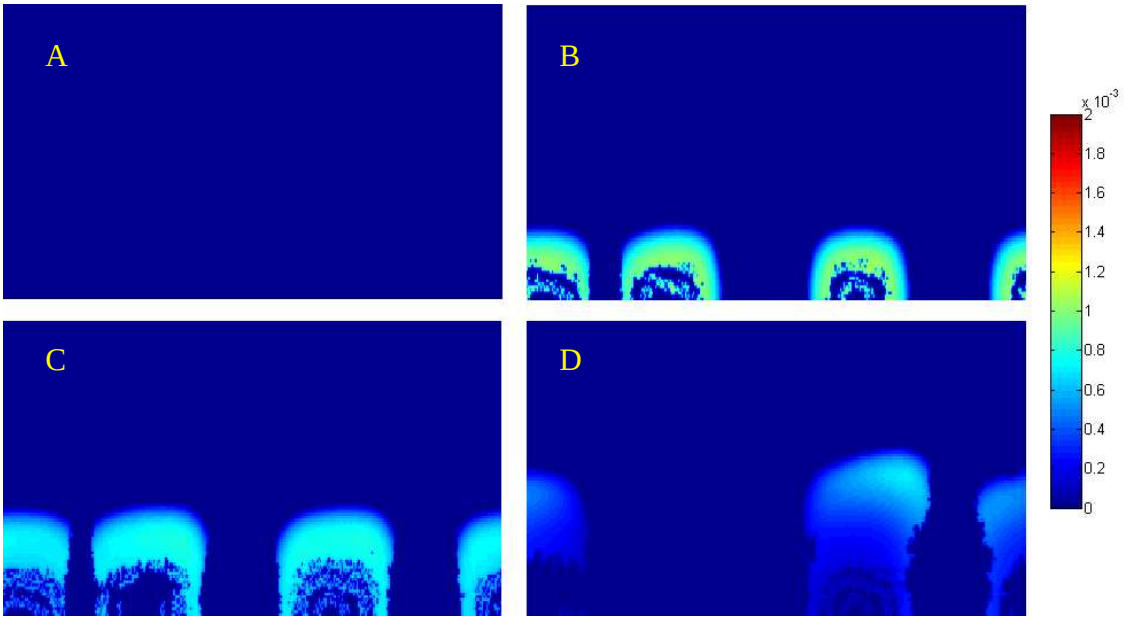

Figure 4c: Nitric oxide accumulation during a simulation of 150 hours with three initially randomly placed bacteria. The left and right borders are continuous. Panel A, B, C and D picture the biofilm after 50, 75, 100 and 143 hours respectively, following colonization. The bar to the right indicates nitric oxide concentration in grams per cubic meter. The parameters under consideration were the survival threshold, survival time limit, nitric oxide reduction constant and respiration switch threshold. These were set to $1.5*10^{-15}$, 1, 0.3 and 1 respectively.

No nitric oxide could be observed during the first hours of the simulation corresponding to Figure 4c. This is reflected in the complete absence of NO after 50 hours (panel A). The absence of nitric oxide from the beginning could be observed in every simulation performed. Similarly, in every simulation, nitric oxide accumulation was observed in each microcolony when it had attained a certain size. The initial appearance of NO always occurred in deepest region of the microcolonies, centrally at the substratum. This is to be expected, since these were the regions that were most oxygen deprived and hence where anaerobic respiration would be carried out.

Another characteristic of NO accumulation observed in all simulations performed was that nitric oxide always appeared in an initial burst of higher concentration, which subsequently receded to lower concentration as NO extended upwards and outwards (sideways) in the microcolonies. This can be seen by comparing panel B, C and D in Figure 4c.

In Figure 4d, the accumulation of cellular damage in the biofilm in Figure 4a is illustrated.

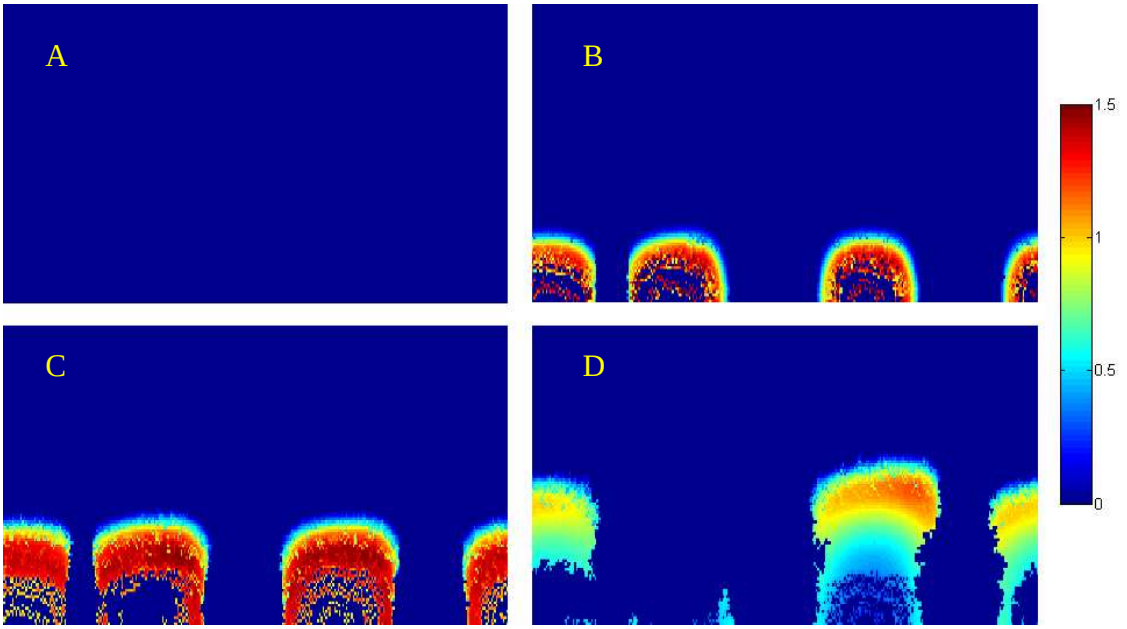

Figure 4d: Damage accumulation during a simulation of 150 hours with three initially randomly placed bacteria. The left and right borders are continuous. Panel A, B, C and D picture the biofilm after 50, 75, 100 and 143 hours respectively, following colonization. The bar to the right indicates the amount of damage in 10^{-15} "grams". The parameters under consideration were the survival threshold, survival time limit, nitric oxide reduction constant and respiration switch threshold. These were set to $1.5*10^{-15}$, 1, 0.3 and 1 respectively.

The panels in Figure 4d display three common characteristics of damage accumulation that could be observed in all simulations performed. First, biofilms suffered no damage during the first hours of the simulation. This is reflected in the absence of damage in panel A of Figure 4d. Second, initial damage accumulation always appeared centrally in the microcolonies, at the substratum. By comparing panel B and C in Figure 4d with their respective panels in Figure 4a, it can be seen that the damage is centered in the deepest regions of the biofilm. The third feature was that the damage sustained by the bacteria was most severe in the initial stages of damage accumulation. Over time, damage receded to lower levels. The distribution of damage also changed such that the highest level of damage continuously appeared in higher regions of the microcolonies as they grew taller. These observations can be seen by comparing the difference in damage severity and distribution between panel C and D in Figure 4d. By comparing the panels in Figure 4d with those in Figure 4c, the damage can be seen to correlate with the levels of nitric oxide in the microcolonies. Damage accumulation was followed by cell death and hollowing in the majority of simulations performed.

3.2 Comparison to experimental observations

In order to evaluate the predictions of the model, the results obtained from the simulations performed were compared to experimental data [3, 21, 23, 24, 26, 27]. From these studies, one can recognize two distinct variations of the hollowing process. In the first variant, voids form centrally in the microcolonies, at the substratum [3, 23, 26].

Following extensive cell death, large parts of the microcolonies detach from the substratum, leaving only a few live cells attached [23]. The second variant also involves voids forming centrally in the microcolonies. The difference is that these voids appear higher in the microcolonies, above the substratum [21, 23, 24, 27]. The voids eventually open upwards, allowing cells in the interior of the microcolonies to disperse [21].

As mentioned in section 3.1, the present model uniformly predicted initial void formation centrally in the microcolonies at the substratum; in the simulations that hollowing was observed. Since oxygen depletion is most severe in these regions, this is where anaerobic respiration will utilized to the greatest extent. Anaerobic respiration leads to nitric oxide production, and when the production outweighs the reduction, NO will accumulate. The nitric oxide will subsequently cause cellular damage accumulation if NO reaches high enough levels to outweigh the damage reduction. When the damage becomes severe enough, the bacteria die.

When considering the above results in light of experimentally observed hollowing, it can be concluded that the model predictions are in agreement with the first variant of void formation. The pattern of hollowing reported in [3, 26] shows spatial similarity that predicted by the model. Although the initial void formation observed in [23] followed the second variant of hollowing, subsequently reported cell death showed similarity to the model predictions. In addition, the model also captured the experimentally observed presence of live cells in the voids [3, 23] and sloughing of most of the microcolonies as a result of extensive cell death [23]. From this it can be inferred that, according to the predictions of the model, nitric oxide accumulation and the resulting damage can account for the first variant of hollowing.

By comparing the model results to [21, 24, 27], however, it can be concluded that the model was not been able to capture the pattern of void formation observed in these studies. Because the model always predicts that oxygen depletion is most severe in the deepest regions of the microcolonies, nitric oxide and damage accumulation initially occurs in these regions. Based on this it can be concluded that mechanism of hollowing investigated by the present model cannot account for the second variant of void formation. One mechanism for cell death that has been shown to be involved in this form of hollowing is the production of an autotoxic protein called AlpP [23].

3.3 Quantitative data

In this section, quantitative data from the simulations run with the chosen parameter value combinations will be presented. These simulations were run with force-placed bacteria to facilitate comparison of the results. The information given includes the timing of initial void formation and sloughing, if it occurred. In the cases where no hollowing and sloughing was observed, the peak of damage or death counter measurement was included. Table 2 covers the data from simulations run with the respiration switch threshold set to 0.5.

Table 2: Timing of initial void formation and sloughing event for simulations run with the respiration switch threshold equal to 0.5.

Survival threshold	Survival time limit	NO reduction constant	Initial void formation (h)	Initial sloughing (h)	Damage/Death counter top
$0.5*10^{-15}$	1	0.1	62	102	-
$1*10^{-15}$	1	0.1	61	98	-
$1.5*10^{-15}$	1	0.1	62	93	-
$0.5*10^{-15}$	20	0.1	80	96	-
$1*10^{-15}$	20	0.1	80	99	-
$1.5*10^{-15}$	20	0.1	81	121	-
$0.5*10^{-15}$	40	0.1	100	115	-
$1*10^{-15}$	40	0.1	101	116	-
$1.5*10^{-15}$	40	0.1	101	118	-
$0.5*10^{-15}$	1	0.3	63	102	-
$1*10^{-15}$	1	0.3	65	136	-
$1.5*10^{-15}$	1	0.3	62	145	-
$0.5*10^{-15}$	20	0.3	81	102	-
$1*10^{-15}$	20	0.3	84	134	-
$1.5*10^{-15}$	20	0.3	91 [a]	-	15-20
$0.5*10^{-15}$	40	0.3	101	128	-
$1*10^{-15}$	40	0.3	-	-	25-30
$1.5*10^{-15}$	40	0.3	-	-	15-20
$0.5*10^{-15}$	1	0.5	65	99	-
$1*10^{-15}$	1	0.5	-	-	0.8
$1.5*10^{-15}$	1	0.5	-	-	0.9-0.95
$0.5*10^{-15}$	20	0.5	85	125	-
$1*10^{-15}$	20	0.5	-	-	0
$1.5*10^{-15}$	20	0.5	-	-	0
$0.5*10^{-15}$	40	0.5	-	-	25-30
$1*10^{-15}$	40	0.5	-	-	0
$1.5*10^{-15}$	40	0.5	-	-	0

Each row represents one simulation. Damage was included for simulations that did not show any void formation and sloughing event, and had the survival time limit set to one. Death counter measurements were given for simulations that showed no hollowing or sloughing, and had a survival time limit greater than one. The intervals for damage and death counter measurements indicate the closest estimates made from visual inspection of the results.
[a]Only barely showed void formation

In Table 3, data from simulations run with the respiration switch threshold equal to one can be seen.

Table 3: Timing of initial void formation and sloughing event for simulations run with the respiration switch threshold equal to one.

Survival threshold	Survival time limit	NO reduction constant	Initial void formation (h)	Initial sloughing (h)	Damage/Death counter top
$0.5*10^{-15}$	1	0.1	56	97	-
$1*10^{-15}$	1	0.1	56	90	-
$1.5*10^{-15}$	1	0.1	57	105	-
$0.5*10^{-15}$	20	0.1	75	102	-
$1*10^{-15}$	20	0.1	75	92	-
$1.5*10^{-15}$	20	0.1	76	104	-
$0.5*10^{-15}$	40	0.1	95	109	-
$1*10^{-15}$	40	0.1	95	110	-
$1.5*10^{-15}$	40	0.1	96	112	-
$0.5*10^{-15}$	1	0.3	57	95	-
$1*10^{-15}$	1	0.3	60	98	-
$1.5*10^{-15}$	1	0.3	62	-	-
$0.5*10^{-15}$	20	0.3	79	108	-
$1*10^{-15}$	20	0.3	81	118	-
$1.5*10^{-15}$	20	0.3	-	-	15-20
$0.5*10^{-15}$	40	0.3	97	112	-
$1*10^{-15}$	40	0.3	-	-	25-30
$1.5*10^{-15}$	40	0.3	-	-	15-20
$0.5*10^{-15}$	1	0.5	60	88	-
$1*10^{-15}$	1	0.5	-	-	0.9-0.95
$1.5*10^{-15}$	1	0.5	-	-	0.9-0.95
$0.5*10^{-15}$	20	0.5	80	94	-
$1*10^{-15}$	20	0.5	-	-	0
$1.5*10^{-15}$	20	0.5	-	-	0
$0.5*10^{-15}$	40	0.5	-	-	25-30
$1*10^{-15}$	40	0.5	-	-	0
$1.5*10^{-15}$	40	0.5	-	-	0

Each row represents one simulation. Damage was included for simulations that did not show any void formation and sloughing event, and had the survival time limit set to one. Death counter measurements were given for simulations that showed no hollowing or sloughing, and had a survival time limit greater than one. The intervals for damage and death counter measurements indicate the closest estimates made from visual inspection of the results.

Table 4 gives the data from the simulations run with the respiration switch threshold set to 1.5.

Table 4: Timing of initial void formation and sloughing event for simulations run with the respiration switch threshold equal to 1.5.

Survival threshold	Survival time limit	NO reduction constant	Initial void formation (h)	Initial sloughing (h)	Damage/Death counter top
$0.5*10^{-15}$	1	0.1	52	89	-
$1*10^{-15}$	1	0.1	53	107	-
$1.5*10^{-15}$	1	0.1	54	82	-
$0.5*10^{-15}$	20	0.1	73	89	-
$1*10^{-15}$	20	0.1	71	89	-
$1.5*10^{-15}$	20	0.1	72	90	-
$0.5*10^{-15}$	40	0.1	90	107	-
$1*10^{-15}$	40	0.1	91	106	-
$1.5*10^{-15}$	40	0.1	94	109	-
$0.5*10^{-15}$	1	0.3	59	88	-
$1*10^{-15}$	1	0.3	58	93	-
$1.5*10^{-15}$	1	0.3	62	-	-
$0.5*10^{-15}$	20	0.3	75	92	-
$1*10^{-15}$	20	0.3	77	97	-
$1.5*10^{-15}$	20	0.3	-	-	15-20
$0.5*10^{-15}$	40	0.3	95	126	-
$1*10^{-15}$	40	0.3	-	-	25-30
$1.5*10^{-15}$	40	0.3	-	-	15-20
$0.5*10^{-15}$	1	0.5	58	94	
$1*10^{-15}$	1	0.5	-	-	0-9-0.95
$1.5*10^{-15}$	1	0.5	-	-	0.9-0.95
$0.5*10^{-15}$	20	0.5	77	103	-
$1*10^{-15}$	20	0.5	-	-	0
$1.5*10^{-15}$	20	0.5	-	-	0
$0.5*10^{-15}$	40	0.5	-	-	20-25
$1*10^{-15}$	40	0.5	-	-	-
$1.5*10^{-15}$	40	0.5	-	-	-

Each row represents one simulation. Damage was included for simulations that did not show any void formation and sloughing event, and had the survival time limit set to one. Death counter measurements were given for simulations that showed no hollowing or sloughing, and had a survival time limit greater than one. The intervals for damage and death counter measurements indicate the closest estimates made from visual inspection of the results.

Based on the data in Table 2, 3 and 4, several conclusions can be made. By comparing the simulations in each table with respect to survival time limit, it can be seen that higher limit corresponds to later timing of initial void formation. This is to be expected, since a high time limit means that the bacteria must sustain a certain amount of damage for a longer time. Simulations with a time limit of twenty showed initial hollowing approximately twenty hours later than those with the limit equal to one. The same delay was not found for initial sloughing, however. While higher time limit generally delayed sloughing, it is not to the same extent as void formation. This means that the time frame between initial hollowing and sloughing is smaller for simulations with higher time limit. In other words, the progression of hollowing was more rapid in these cases (cell death

was more frequent). The reason for this is suggested to be that, while cell death ensued later, damage had accumulated throughout the biofilm at the time of initial hollowing. Once the void formation commenced, it proceeded more swiftly through the microcolonies.

Another observation is that, for simulations with higher NO reduction constant and survival time limit, sloughing and hollowing did not occur. This is because the damage accumulation never becomes severe enough to cause cell death. Higher respiration switch threshold appears to slightly delay both initial void formation and sloughing.

4 Conclusion

The most relevant result obtained in this study is the uniform prediction by the model that voids form centrally in the microcolonies, at the substratum. This pattern of hollowing is in agreement with some experimental data [3, 23, 26], but not others [21, 23, 24, 27]. From this it can be concluded that the model results supports the hypothesis that nitric oxide is a factor involved in the pattern of hollowing observed in [3, 23, 26]. It can also be inferred that other mechanisms must be involved to explain the void formation reported in [21, 23, 24, 27].

From an evolutionary perspective, starvation-mediated sloughing makes sense. This is because nutrient depletion could then serve as a signal to the bacteria to detach and colonize other surfaces where there are more nutrients. As the top part of the biofilm detaches, the lower regions can regain access to higher levels of substrate and grow into new microcolonies.

5 Future work

Although the predicted features of biofilm development show agreement to reality, the timing of void formation and sloughing is much more uncertain. The low confidence of timing prediction can be attributed to the fact that the vital parameter values responsible for cell death have not been experimentally determined. If it would be possible to determine realistic values for these parameters, the model could be used to more accurately predict the pattern and timing of cell death in biofilms.

Another future prospect would be to develop the model further by taking additional processes into consideration. Two such processes could be the role of nitric oxide in cell dispersal [26] and nutrient release from dead cells [4].

A pitfall that was faced during the development of the model was time-consuming problems with molecular diffusion. The main cause of these problems was determined to be instability in the diffusion function, resulting from inappropriate parameter values involved in the discretization of diffusion. Instability involved oscillation of the substrate concentration gradients. One possible trigger for instability was a rapid change in the gradient, caused by sloughing.

6 Acknowledgements

The author wishes to thank the people at the School of Life Sciences at Skövde University of Sweden, in particular Magnus Fagerlind, Andreas Jansson and Patric Nilsson, for their assistance with this project. Additional thanks goes to Nicolas Barraud at the School of Biotechnology and Biomolecular Sciences at the University of New South Wales for his valuable inputs.

7 References

[1] O'Toole G., Kaplan H. B., Kolter R. (2000) Biofilm formation as microbial development. *Annual Review of Microbiology, 54*, 49-79.

[2] Madigan M. T. & Martinko J. M. (2006) *Biology of Microorganisms*. Pearson Prentice Hall.

[3] Webb J. S., Thompson L. S., James J., Charlton T., Tolker-Nielser T., Koch B., Givskov M., Kjelleberg S. (2003) Cell death in *Pseudomonas aeruginosa* biofilm development. *Journal of Bacteriology, 185*, 4585-4592.

[4] Webb J. S., Givskov M., Kjellberg S. (2003) Bacterial biofilms: prokaryotic adventures in multicellularity. *Current Opinion in Microbiology, 6*, 578-585.

[5] Sauer K., Cullen M. C., Rickard A. H., Zeef L. A. H., Davies D. G., Gilbert P. (2004) Characterization of nutrient-induced dispersion in *Pseudomonas aeruginosa* PAO1 Biofilm. *Journal of Bacteriology, 186*, 7312-7326.

[6] Picioreanu C., van Loosdrecht M. C. M., Heijnen J. J (2000) Two-dimensional model of biofilm detachment caused by internal stress from liquid flow. *Biotechnology and Bioengineering, 72*, 205-218.

[7] Rice S. A., Koh K. S., Queck S. Y., Labbate M., Lam K. W., Kjelleberg S. (2005) Biofilm formation and sloughing in *Serratia marcescens* are controlled by quorum sensing and nutrient cues. *Journal of Bacteriology, 187*, 3477-3485.

[8] Davey M. E., Caiazza N. C., O'Toole G. A. (2002) Rhamnolipid surfacant Production affects biofilm architecture in *Pseudomonas aeruginosa* PAO1. *Journal of Bacteriology, 185*, 1027-1036.

[9] Gjermansen M, Ragas P., Sternberg C., Molin S., Tolker-Nielsen T. (2005) Characterization of starvation-induced dispersion in *Pseudomonas putida* biofilms. *Environmental Microbiology, 7*, 894-904.

[10] Costerton, J. W., Stewart P. S., Greenberg E. P. (1999) Bacterial biofilms: a common cause of persistent infections. *Science, 284,* 1318–1322.

[11] Piriou P., Dukan S., Levi Y., Jarrige P. A. (1997) Prevention of bacterial growth in drinking water distribution systems. *Water Science and Technology, 35,* 283–287.

[12] Parsek M. R. & Fuqua C. (2004) Biofilms 2003: Emerging themes and challenges in studies of surface-associated microbial life. *Journal of Bacteriology, 186,* 4427-4440.

[13] Kreft J-U., Piciorenau C., Wimpenny J. W. T., van Loosdrecht M. C. M. (2001) Individual-based modeling of biofilms. *Microbiology ,147,* 2897-2912.

[14] Wimpenny J. W. T., Colasanti R. (1997) A unifying hypothesis for the structure of microbial biofilms based on cellular automaton models. *FEMS Microbiology Ecology, 22,* 1-16.

[15] Picioreanu C., van Loosdrecht M. C. M., Heijnen, J. J. (1998) A new combined differential-discrete cellular automaton approach for biofilm modeling: application for growth in gel beads. *Biotechnology and Bioengineering, 57,* 718-731.

[16] Hermanowicz S. W. (1999) Two-dimensional simulations of biofilm development: Effects of external environmental conditions. *Water Science and Technology, 39,* 107-114.

[17] Ermentrout G. B., Edelstein-Keshet L. (1993) Cellular automata approaches to biological modeling. *Journal of Theoretical Biology, 160,* 97-133.

[18] DeAngelis D. L., & Gross L. J. (1992) *Individual-based models and approaches in ecology: populations, communities, and ecosystems*. New York: Chapman and Hall.

[19] Chang I., Gilbert E. S., Eliashberg N., Keasling J. D. (2003) A three-dimensional, stochastic simulation of biofilm growth and transport-related factors that affect structure. *Microbiology, 149,* 2859-2871.

[20] Auschill T. M., Artweiler N. B., Netuschil N., Brecx M., Reich E., Sculean A. (2000) Spatial distribution of vital and dead microorganisms in dental biofilms. *Archives of Oral Biology, 46,* 471-476.

[21] Sauer K., Camper A. K., Ehrlich G. D., Consterton J. W., Davies D. G. (2001) *Pseudomonas aeruginosa* displays multiple phenotypes during development as a biofilm. *Journal of Bacteriology, 184,* 1140-1154.

[22] Tolker-Nielsen T., Brinch U. C., Ragas R. C., Andersen J. B., Jacobsen C. S., Molin S. (2000) Development an dynamics of *Pseudomonas* sp. Biofilms. *Journal of Bacteriology, 182,* 6482-6489.

[23] Mai-Prochnow A., Evans F., Dalisay-Saludes D., Stelzer S., Egan S., James S., Webb J. S., Kjelleberg S. (2004) Biofilm development and cell death in the marine bacterium *Pseudoalteromonas tunicata*. *Applied and Environmental Microbiology, 70,* 3232–3238.

[24] Hunt S. M., Werner E. M., Huang B., Hamilton M. A., Stewart P. S. (2004) Hypothesis for the role of nutrient starvation in biofilm detachment. *Applied and Environmental Microbiology, 70,* 7418-7425.

[25] Hunt S. M., Hamilton M. A., Sears J. T., Harkin G., Reno J. (2003) A computer investigation of chemically mediated detachment in bacterial biofilms. *Microbiology, 149,* 1155-1163.

[26] Barraud N., Hassett D. J., Hwang S-H., Rice S. A., Kjellberg S., Webb J. S. (2006) Involvement of nitric oxide in biofilm dispersal. *American Society of Microbiology, 188,* 7344-7353.

[27] Purevdorj-Gage B., Costerton W. J., Stoodley P. (2005) Phenotypic differentiation and seeding dispersal in non-mucoid and mucoid *Pseudomonas aeruginosa* biofilms. *Microbiology, 151,* 1569-1576.

[28] Characklis W. G. (1989) *Biofilms* (p. 55-89, 114). Edited by Characklis W. G. and Marshall K. C. New York: Wiley.

[29] Chen F., Xia Q., Ju L-K. (2006) Competition Between oxygen and nitrate respirations in continuous culture of *Pseudomonas aeruginosa* performing aerobic denitrification. *Biotechnology and Bioengineering, 93,* 1069-1078.

[30] Edelstein-Keshet L. (1988) *Mathematical Models in Biology* (p. 275-279). McGraw-Hill.

[31] Stewart P. S. (2003) Diffusion in biofilms. *Journal of Bacteriology, 185,* 1485-1491.

[32] Picioreanu C., van Loosdrecht M. C. M., Heijnen J. J. (1999) Discrete-differential modeling of biofilm structure. *Water Science and Technology, 39,* 115-22.

[33] De Beer D. P., Stoodley F. R., Lewandowski Z. (1994) Effects of biofilm structures on oxygen distribution and mass transport. *Biotechnology and Bioengineering, 43,* 1131-1138.

[34] Picioreanu C., van Loosdrecht M. C. M., Heijnen J. J. (1997) A new combined differential-discrete cellular automaton approach for biofilm modeling: application for growth in gel beds. *Biotechnology and Bioengineering,57,* 718-731.

[35] Hermanowicz S. (2000) A simple 4d biofilm model yields a variety of morphological features. *Mathematical Biosciences, 169,* 1-14.

[36] Sternberg C, Christensen B. B., Johansen T., Toftgaard Nielsen A., Andersen J. B., Givskov M., Molin S. (1999) Distribution of bacterial growth activity in flow-chamber biofilms. *Applied and Environmental Microbiology, 65*, 4108-4117.

[37] Chen B., Keshive M., Deen W. M. (1998) Diffusion and reaction of nitric oxide in suspension cell cultures. *Biophysical Journal, 75*, 745-754.

[38] Shaler T. A. & Klecka G. M. (1986) Effects of dissolved oxygen concentration on biodegradation of 2,4-dichlorophenoxyacetic acid. *Applied and Environmental Miocrobiology, 51*, 950-955.

[39] Kreft J. U., Booth G., Wimpenny J. W. T. (1998) BacSim, a simulator for individual-based modeling of bacterial colony growth. *Microbiology, 144*, 3275-3287.

[40] Betlach M. R., Tiedje J. M. (1981) Kinetic explanation for accumulation of nitrite, nitric oxide and nitrous oxide during bacterial denitrification. *Applied and Environmental Microbiology, 42*, 1074-1084.